Title

The negative triangularity tokamak: stability limits and prospects as a fusion energy system

Journal

Nuclear Fusion, 55(6)

ISSN

0029-5515

Authors

Medvedev, S Yu
Kikuchi, M
Villard, L
et al.

Publication Date

2015-06-01

DOI

10.1088/0029-5515/55/6/063013

Peer reviewed

Author's final version
Published as:
Nucl. Fusion **55**, 063013, 2015
http://dx.doi.org/10.1088/0029-5515/55/6/063013

Negative triangularity tokamak: stability limits and perspectives as fusion energy system

S Yu Medvedev[1,2], M Kikuchi[3], L Villard[4], T Takizuka[5], P Diamond[6], H Zushi[7], K Nagasaki[8], X Duan[9], Y Wu[10], A A Ivanov[1], A A Martynov[1], Yu Yu Poshekhonov[1], A Fasoli[4], O Sauter[4]

[1]Keldysh Institute of Applied Mathematics, RAS, Moscow, Russia, [2]National Research Nuclear University MEPhI, Moscow, Russia, [3]Japan Atomic Energy Agency, Naka, Japan, [4]CRPP-EPFL, Lausanne, Switzerland, [5]Osaka University, Osaka, Japan, [6]UCSD, San Diego, USA, [7]Kyushu University, Fukuoka, Japan, [8]Kyoto University, Kyoto, Japan, [9]Southwestern Institute of Physics, Chengdu, China, [10]Institute of Nuclear Energy Safety Technology, CAS, Hefei, China

E-mail*:* medvedev@a5.kiam.ru

Abstract. The paper discusses edge stability, beta limits and power handling issues for negative triangularity tokamaks. The edge MHD stability is the most crucial item for the power handling. For the case of negative triangularity the edge stability picture is quite different from that for conventional positive triangularity tokamaks: the 2nd stability access is closed for localized Mercier/ballooning modes due to the absence of magnetic well, and nearly internal kink modes set the pedestal height limit weakly sensitive to diamagnetic stabilization just above the margin of localized mode Mercier criterion violation. While negative triangularity tokamak is thought to have low beta limit with its magnetic hill property, it is found that plasmas with reactor relevant values of normalized beta $\beta_N > 3$ can be stable to global kink modes without wall stabilization with appropriate core pressure profile optimization against localized mode stability and also with increased magnetic shear in the outer half radius. The beta limit is set by n=1 mode for the resulting flat pressure profile. The wall stabilization is very inefficient due to strong coupling between external and internal modes. The n>1 modes are increasingly internal when approaching the localized mode limit and set a lower beta in case of peaked pressure profile leading to Mercier unstable core. With the theoretical predictions supported by experiments, a negative triangularity tokamak would become a perspective fusion energy system with other advantages including larger separatrix wetted area, more flexible divertor configuration design, wider trapped particle free SOL, lower background magnetic field for internal poloidal field coils and larger pumping conductance from the divertor room.

PACS numbers: 28.52.-s, 52.55.Fa, 52.35.Py

1. Introduction

Negative triangularity tokamak plasmas are subject of an increased interest both in existing experiments and in studies of core physics as well as power handling relevant to fusion demonstration power reactors [1-5]. The plasma shape optimization with positive triangularity tends to lead to the stabilization of high-*n* modes such as ballooning modes through entering into the second stability regime. Then, the limiting edge MHD instabilities become medium-*n* peeling-ballooning and low-*n* peeling modes, which result in severe ELM activity damaging the divertor plates. For the case of negative triangularity, the 2nd stability access is closed for ballooning modes [6]. The destabilization of a whole range of fixed boundary medium- and low-*n* modes takes place for pedestal heights just above the values for which the Mercier criterion for localized modes is violated, implying possible changes in the ELM characteristics as compared to positive triangularity configurations: as a matter of fact, H-mode discharges with upper negative triangularity in TCV demonstrate increased frequency and significant mitigation of type I ELM peak power losses [4]. This is consistent with lower edge stability limits for the pedestal. Double null negative triangularity configurations feature quite high

stable pedestals in the 1st region of ballooning stability provided that the pedestal current density is low. Internal modes (unstable already with fixed boundary condition but localized in the pedestal region) set the pedestal height limit, which is much less sensitive to pedestal profile variations but also to diamagnetic stabilization than conventional peeling-ballooning mode limits [8].

While negative triangularity plasma has some favorable MHD property regarding ELM behavior, the beta limit is relatively low. That is connected with the absence of magnetic well for elongated plasma cross-sections. In Ref. [9] the oblate negative triangularity (comet) plasma cross-section was proposed to restore the magnetic well at negative triangularity but with low-n external kink limited normalized beta value $\beta_N \sim 2$. Recent MHD stability calculations for the negative triangularity plasma extend the investigation of TCV tokamak beta limits and edge stability [6-8] to double null shapes, lower aspect ratio, negative shear and Mercier unstable plasma core. For the case of negative triangularity, a well-defined Mercier/ballooning limiting pressure gradient profile exists under fixed parallel current density or safety factor profiles in the positive shear region. The external kink mode stability limit can be obtained by rescaling the limiting profiles. Negative triangularity tokamak configurations with optimized pressure gradient profiles can be stable for $\beta_N > 3$ at moderate elongation $\kappa = 1.5$ and internal inductance value $l_i = 0.9$, even in the absence of the magnetic well, with Mercier modes stabilized by magnetic shear. However, wall stabilization is very inefficient for such plasmas due to strong coupling between global internal modes and external kink modes. Reverse shear configurations allow for larger pressure gradient in the core stable against localized modes and larger bootstrap current fraction but coupling to infernal modes leads to lower $\beta_N \sim 2$ and further profile optimization is needed. The LHD experiments showed that plasma beta much above Mercier stability limit can be achieved [10]. This suggests that for negative triangularity tokamaks, the pressure gradient in the core as well as in the pedestal might not be limited by localized Mercier modes. It opens more freedom for plasma profile optimization, in particular maximizing bootstrap current fraction.

Apart from ELM mitigation, negative triangularity tokamaks feature other potential advantages for power handling such as a naturally increased separatrix wetted area and a more flexible divertor configuration using poloidal (PF) coils made of *NbTi* superconductor inside the toroidal field coil in the low field region [3]. Negative triangularity experiments in TCV [11] show a reduction in electron heat transport by a factor of two compared with positive triangularity D-shaped configurations, which is partly explained by nonlinear gyrokinetic simulations [12]. This configuration also allows the inboard ECRF launching to have higher density limit for the ECRF propagation and better pumping accessibility due to larger conductance [3]. The SOL width may also be modified especially in the case of double null configuration with almost vertical magnetic surfaces at the low field side [2].

The remainder of this paper is structured as follows. In section 2, negative triangularity shaped tokamaks are examined from the point of view of their power handling capabilities. The magnetic well properties and their link to localized mode stability are presented in section 3. Beta limits are studied in section 4, examining various profiles and also oblate cross-sections. Edge stability of negative triangularity plasmas is examined in section 5 and vertical stability in section 6. Discussion and conclusions are presented in section 7.

2. Perspectives as fusion energy system

To reconcile a challenging situation with power handling, a large reduction in the heat flux compared with the standard D-shaped X-point divertor tokamak would be needed. The proposed tokamak configuration with strong negative triangularity provides a possible operating scenario [2]. Standard first stability tokamak reactor designs [13] such as steady state tokamak reactor (SSTR) or ARIES-I utilize moderate normalized beta ($\beta_N = 3.2 - 3.5$) and the "core-the-first" design philosophy – optimization for the core confinement with many drawbacks for the power handling in the fusion power system, which leads to an excessive uncontrolled heat flux up to $\sim 70\ MW/m^2$, close to the radiation heat flux at the surface of the Sun. Even with a sophisticated radiative cooling scheme in the core and the edge, the typical heat flux is $\sim 10\ MW/m^2$ [14]. Since the maximum heat fluxes for conventional power plants are $\sim 0.3\ MW/m^2$ for coal-fired plants and $\sim 1\ MW/m^2$ for fission plants, such high steady state heat flux casts a doubt on the operational reliability of the fusion power station,

even if a plasma facing component is developed to withstand such a high heat flux. While a significant effort has been made to realize such a divertor control during the last two decades, no good success has been reached with the standard "core-the-first" design. The use of snowflake (SF-divertor) has been proposed to expand the heat flux width more than in standard X-point divertor tokamak by a factor of $F = 1.5 – 3$ [15-16], but this configuration requires too large PF coil currents for the standard D-shaped tokamak reactor. Recent studies [17] show that internal poloidal field coils are necessary to realize the snowflake configuration and the required Ampere-turn value is higher than 100 *MA*t* for the plasma current of 16.7 *MA*.

The strongly D-shaped plasma leads to the divertor position to have smaller major radius than the plasma major radius, $R_{div} < R_p$, and the heat flux at the divertor plates is correspondingly enhanced. Accordingly, some countermeasures to reduce the transient and steady divertor heat loads in a tokamak reactor should be adopted such as the resonant magnetic perturbation (RMP) [18] and the pellet pace-making [19] for the ELM and the enhanced radiative-cooling in the core and the edge plasmas, while RMP may produce lobe structure (homoclinic tangle) [20] near the separatrix and induce 3D heat flux problem.

Three geometries are shown in figure 1 with a positive triangularity ($\delta = 0.8$) single null (SN) (figure 1a), a negative triangularity $\delta = –0.8$ with SF-divertor (figure 1b) and a negative triangularity ($\delta = –0.9$) double null (DN) (figure 1c); $R_p = 7$ *m*, $A = R_p/a_p = 2.6$. With positive triangularity, the divertor position is $R_{div}(\delta>0) = 4.0$ *m*. On the other hand, $R_{div}(\delta<0) = 10.0$ *m*. The power handling area for the divertor is $S_{div} \sim 2\pi R_{div}$ ($F\Delta$), where Δ is effective width of the heat flux at the divertor plate for a standard X-point configuration including the effect of inclination of the divertor target, and F is the enhancement factor due to the SF flux expansion. Since $R_{div}(\delta<0)/R_{div}(\delta>0) = 2.5$ and $F = 1.5–3$ is expected [16], negative triangularity SF-divertor tokamak may have an effective area enhancement 4 – 7 over the standard D-shaped tokamak. If such an enhancement factor is realized, the solution to the power handling in the tokamak reactor may be technically more feasible by changing the uncontrolled heat flux from 70 MW/m^2 to 10 MW/m^2. To achieve the heat flux $q_{div} \sim 10$ MW/m^2 at $R_{div} = 10$ *m*, the heat flux width has to be $F\Delta \sim 0.5$ *m*. Negative triangularity DN may also have such an enhancement factor but has issues related to the axisymmetric instability and the reduction of the tritium breeding ratio (TBR) due to the reduction of the coverage of the blanket, while there are some merits.

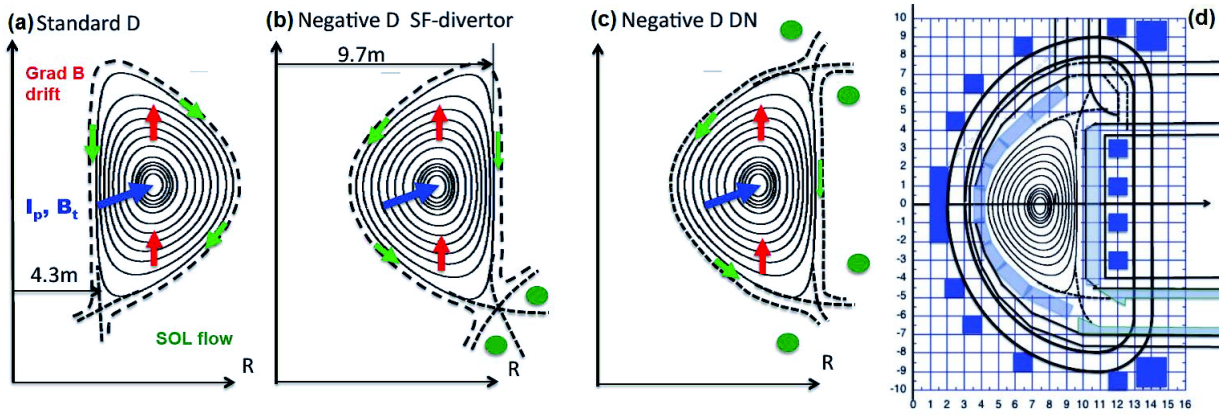

Figure 1. Equilibrium configurations and SOL flow patterns for (a) standard D-shaped tokamak, (b) negative triangularity SF-divertor tokamak, (c) negative triangularity DN tokamak (∇B drift away from X-point for SN cases), and (d) magnetic system for negative triangularity DN with internal PF coils.

Two obvious merits of the negative triangularity tokamak are: 1) lower background magnetic field for internal poloidal field coils and 2) larger pumping conductance from the divertor room. Other reactor studies such as slim central solenoid (CS) for implementing snowflake divertor [17] show that it is necessary to place the snowflake shaping coils inside the toroidal field coils. With or without snowflake, it is also true that the internal poloidal field coil system makes the divertor configuration robust against plasma perturbations. Then there is a significant merit for the negative triangularity

tokamak, since B_t is much weaker at the snowflake shaping coils and *NbTi* superconductors can be used for the shaping coils. At high background magnetic field, use of Nb_3Sn superconductor is necessary and the wind-and-react on machine has a lot of technical issues. In case of *NbTi*, it is quite robust against bending and much better suited for the internal poloidal field coils. Figure 1d demonstrates that radiation shielding for superconducting coil system with a thickness ~1m can be compatible with the PF coil design. In the standard D-shaped tokamak reactor design such as SSTR, the pumping duct design is a difficulty since thick 14 *MeV* neutron shielding reduces the net pumping conductance from the inboard divertor room. In case of negative triangularity, the divertor room is in the outboard side, where there is a wider slot for horizontal and vertical pumping ducts. Without snowflake, pumping duct design is even easier. Periodic replacement of the divertor cassette may be much easier as well.

3. Magnetic well and localized mode stability

The depth of magnetic well is a figure of merit for magnetic confinement system optimization related to localized pressure driven mode stability [21]. The ideal MHD Mercier stability criterion $1/4 - D_M > 0$ [22] provides a constructive definition of a magnetic well parameter $d_m = D_M S^2/\alpha$, where $S = 2V(dq/dV)/q$ is the magnetic shear and $\alpha = 2\mu_0(dp/d\Psi)(dV/d\Psi)\sqrt{V/(2\pi^2 R_0)}/(4\pi^2)$ is the normalized pressure gradient, and V is the volume enclosed by magnetic surface $\Psi = const$. Negative values of d_m corresponds to the existence of a magnetic well, and a weak shear and/or large absolute values of d_m provide 2nd stability access for high-*n* ballooning modes [23]. On the opposite, positive values of d_m mean that localized mode stabilization is only possible with finite shear and the 2nd stability access is closed. Larger values of safety factor q lead to restoration of the magnetic well despite unfavorable geometrical properties of the magnetic field geometry.

The dependence of magnetic well on the plasma cross-section shaping was the subject of an analysis in Refs. [24, 25]. In the vicinity of magnetic axis the following relation holds for a critical value of the axis safety factor q_0 beyond which the magnetic well is established:

$$q_0^2 > \frac{1}{1 - 3\dfrac{(\kappa^2 - 1)(\kappa^2 - 2\delta/\varepsilon)}{(3\kappa^2 + 1)(\kappa^2 + 1)}}, \qquad (1)$$

where κ is the tokamak plasma cross-section elongation, δ is the triangularity and ε is the inverse aspect ratio. It readily follows from the condition (1) that the magnetic well near magnetic axis exists for $q_0 \sim 1$ if either $\kappa > 1$ and $\delta > \kappa^2\varepsilon/2$ or $\kappa < 1$ and $\delta < \kappa^2\varepsilon/2$. So either high elongation and large positive triangularity or oblate cross-section and negative triangularity are favourable combinations for the localized mode stability. As mentioned above, the former combination was a general direction of the tokamak plasma optimization, eventually leading to strong type-I ELM crashes. The alternative of comet shape tokamak with oblate (elongation $\kappa < 1$) cross-section and negative triangularity has not demonstrated a potential for high beta plasma stability [9]. On the other hand, the experimental data on enhanced plasma confinement with elongated cross-section and negative triangularity [11] poses a question on the beta limits in the absence of magnetic well.

4. Beta limits

Stability calculations for elongated negative triangularity plasmas in the TCV tokamak showed a beta limit degradation with decreasing triangularity [6]. Beta limits for the reactor scale configuration with R_0 = 7 *m*, a = 2.7 *m* (A = 2.6), κ = 1.5, δ = –0.9 were optimized. The analytic plasma boundary shape with double X-points [26] was used. An iterative procedure was employed to obtain negative triangularity equilibria with ballooning/Mercier optimized pressure profiles [27]. There is no access to the 2nd ballooning stability at all plasma radii, and a well defined limiting pressure gradient

$p' = dp/d\Psi$ exists for fixed profiles of parallel current density $< \mathbf{j}\cdot\mathbf{B} > / < \mathbf{B}\cdot\nabla\varphi >$. Several iterations are sufficient to get self-consistent equilibria with limiting p' profile. A particular case with monotonic q-profile and internal inductance value $l_i = 0.9$ is shown in figure 2a. It gives $\beta_N = \beta[\%]/I_N = 3.4$, $\beta = 2\mu_0 < p >_V / B^2$ for the normalized current $I_N = I_p[MA]/(a[m]B[T]) = 0.9$, $I_p = 15\ MA$, $B = 6.2\ T$ (in figure 2a and in the similar plots further on the dashed lines show the bootstrap current density in the low collision frequency regime and the limiting p' in the corresponding frames). Let us note that the limiting pressure gradient is determined by the Mercier criterion in the plasma core $\sqrt{\psi} < 0.5$, where ψ is the normalized poloidal magnetic flux, and at the very edge of the plasma $\sqrt{\psi} > 0.995$. Elsewhere, localized ballooning modes go unstable while the Mercier criterion is satisfied. The inverse situation is impossible as the Mercier stability is a necessary condition for the ballooning stability [28].

To determine the stability limit against external kink modes, the p' profile is proportionally reduced in a series of fixed boundary equilibria. The stability calculations with the KINX code [29] give $n = 1$ beta limit of $\beta_N = 3.2$ without wall stabilization (lowest value for toroidal mode numbers $n = 1$–5). The corresponding mode structure (level lines and radial profiles of harmonics in straight field line (SFL) flux coordinates for plasma displacement normal to magnetic surfaces) is presented in figures 2b and 2c. The wall stabilization gives very little increase in the beta limit because of strong coupling of internal modes to external kink modes: with the wall proportional to the plasma boundary $a_w/a = 1.3$ $\beta_N = 3.3$ for $n = 1$ mode while for $n > 2$ internal modes set the limit at $\beta_N < 3.5$ very close to the ballooning/Mercier limit. Decreasing shear (lower l_i) leads to lower β_N in accordance with the Mercier criterion in the absence of magnetic well. The result of the ballooning/Mercier pressure gradient optimization for the profiles with bootstrap current in the pedestal and $l_i = 0.75$ is the equilibrium with $\beta_N = 2.7$ (figure 3). The $n = 1$ external kink limit in the equilibria with rescaled pressure profile is $\beta_N = 2.4$ ($\beta_N = 2.6$ with $a_w/a = 1.3$ wall), and the $n > 1$ internal mode limits are very close to the ballooning/Mercier limit. However, the $n = 1$ external kink limit just marginally enhances for higher $l_i = 1.3$ at lower plasma current $I_N = 0.4$ ($q_0 > 1$) with the limiting value $\beta_N = 3.3$.

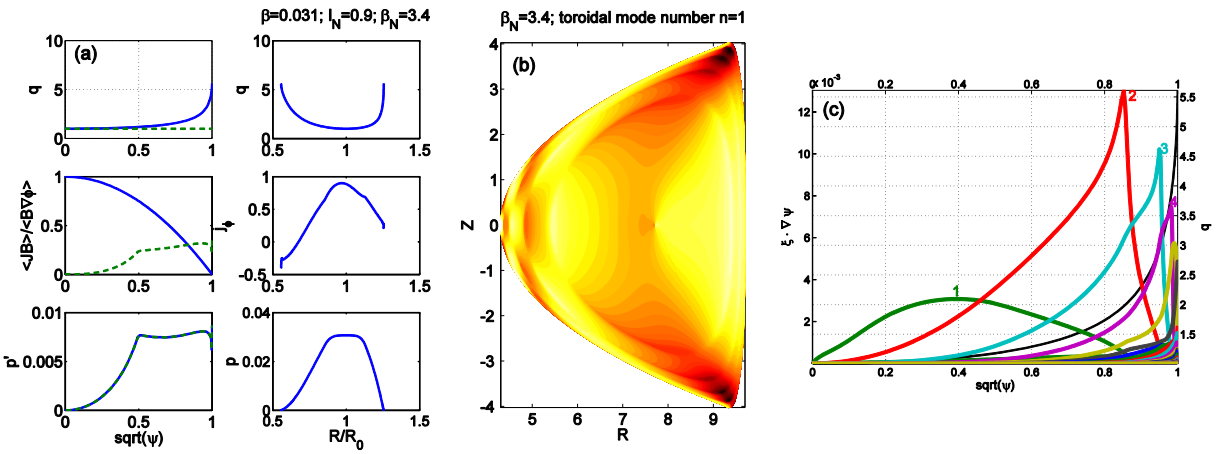

Figure 2. (a) Plasma profiles in the equilibrium with Mercier/ballooning limiting pressure gradient, $l_i = 0.9$, (b) and (c) - the most unstable $n = 1$ mode structure, growth rate $\gamma/\omega_A = 0.003$.

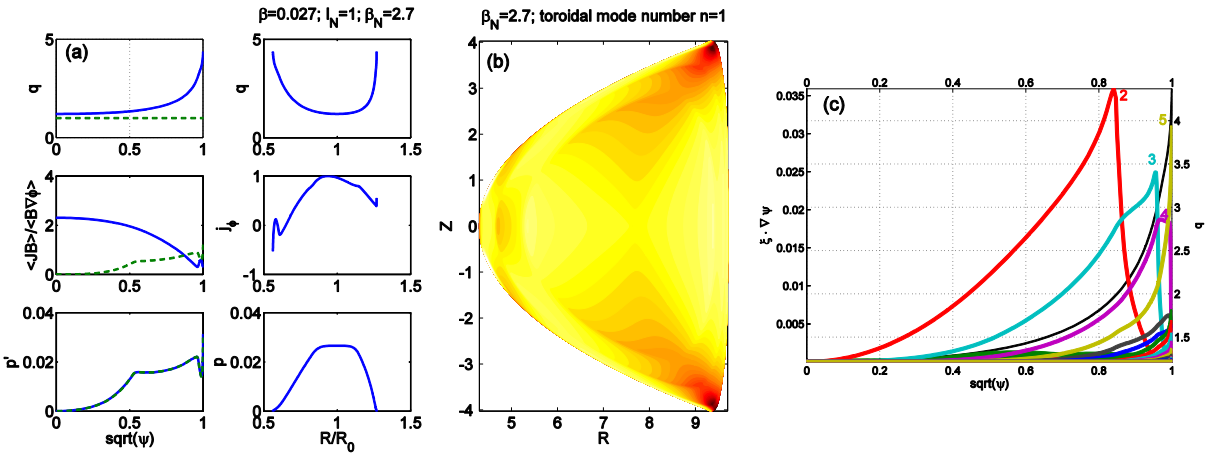

Figure 3. (a) Plasma profiles in the equilibrium with Mercier/ballooning limiting pressure gradient, l_i = 0.75, (b) and (c) - the most unstable n = 1 mode structure, growth rate $\gamma / \omega_A = 0.004$.

The ballooning/Mercier limited case shown in figure 2 features relatively flat pressure profile due to p'=0 at the magnetic axis with the pressure peaking factor $p_0 / < p >$=2.15. The bootstrap current fraction is f_{bs} = 0.7, but the current density is not aligned with the bootstrap current density due to large pressure gradient values at the edge in high shear region. The pressure gradient profile with finite p' at the axis and better alignment near the edge is used to check the sensitivity of beta limits to the pressure profile variations (figure 4). The Mercier criterion is violated in the plasma core, but localized modes are readily stabilized there by kinetic effects under realistic conditions [10, 31]; the pressure peaking is $p_0 / < p >$=2.9 and the bootstrap fraction is f_{bs} = 0.5. The value of normalized current is chosen to be I_N = 0.86 to keep the value of safety factor at the axis q_0 = 1.05. Despite $q_0 > 1$ the n = 1 external mode limited β_N = 2.75 is lower than in the optimized pressure case due to m = 1 mode coupling. Moreover, n > 2 internal modes are driven unstable at β_N = 2.3, well correlated with high-n ballooning mode destabilization in the middle of the plasma, $0.4 < \sqrt{\psi} < 0.8$. The internal n = 5 mode structure is shown in figure 5.

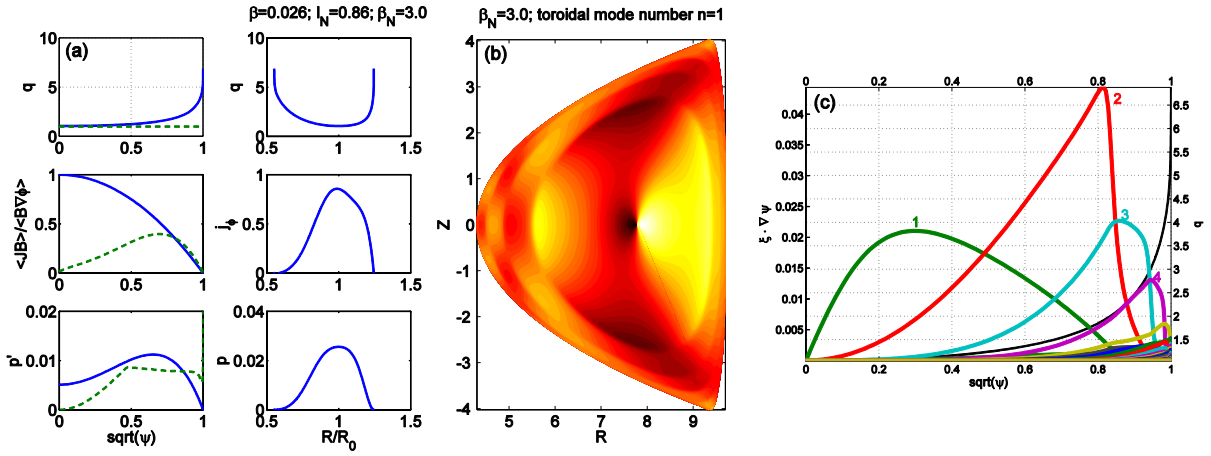

Figure 4. (a) Plasma profiles in the equilibrium with peaked pressure, l_i=0.9, (b) and (c) The most unstable n = 1 mode structure, growth rate $\gamma / \omega_A = 0.01$.

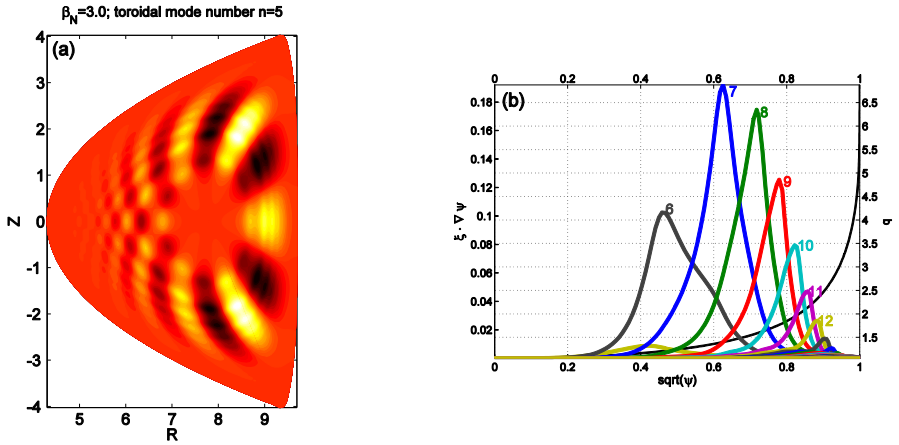

Figure 5. The n = 5 internal mode structure, growth rate $\gamma / \omega_A = 0.049$.

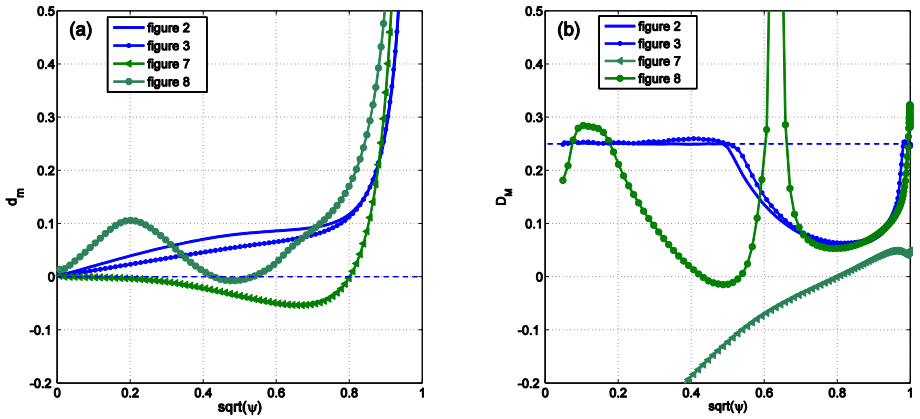

Figure 6. Magnetic well parameter d_m (a) ($d_m < 0$ corresponds to magnetic well) and the Mercier stability term D_M (b) ($1/4 - D_M > 0$ for stability) at magnetic surfaces for DN negative triangularity equilibria (figures 2, 3) and for the oblate cross section (figure 7) and reversed shear cases (figure 8).

The comet shape negative triangularity plasmas with oblate cross-section (elongation $\kappa < 1$) provide a possibility to restore the magnetic well [9] and take an advantage of the good kinetic stabilizing properties of negative triangularity [32] which could be further enhanced at high beta [33]. The DN comet configuration with the same plasma radii but with $\kappa = 0.75$ and $\delta = -0.975$ was used to check a possible enhancement of the beta limit due to better Mercier stability. Indeed the magnetic well exists for $\sqrt{\psi} < 0.8$ but not near the edge (figure 6). In figure 6a the profiles of the magnetic well parameter d_m are shown for the equilibria corresponding to figures 2 and 3 and for the oblate and reversed shear cases presented below. The value of D_M in the Mercier mode criterion $1/4 - D_M > 0$ is given in figure 6b demonstrating that optimized pressure profiles for the elongated equilibria are Mercier limited in the core and at the very edge. In figure 7a ballooning optimized plasma profiles are shown for $I_N = 0.41$ and $q_0 = 1.05$ for the equilibrium with oblate cross section (Mercier modes are stable in the whole plasma). The local ballooning limiting pressure gradient is still over the equilibrium one, indicating the existence of a magnetic well and the 2nd stability access in the plasma core $\sqrt{\psi} < 0.8$. Indeed the pressure peaking for the equilibrium with $\beta_N = 2.8$ is quite high: $p_0 / < p > \; = 3.2$ ($f_{bs} = 0.6$). However, in accordance with [9], the $n = 1$ external kink limit is $\beta_N = 2.0$, while $n > 1$ mode limits coincide with the high-n ballooning limit: $\beta_N < 2.8$. The wall stabilization remains very inefficient: with the ideal wall $a_w/a = 1.3$ the limit is $\beta_N = 2.3$ for the $n = 1$ mode probably due to coupling to both $m = 1$ mode for peaked pressure profile and internal kink modes. On the other hand,

significant enhancement of the axisymmetric n = 0 stability can be expected for the case of oblate plasma cross-section as compared to the elongated negative triangularity plasmas (see section 4).

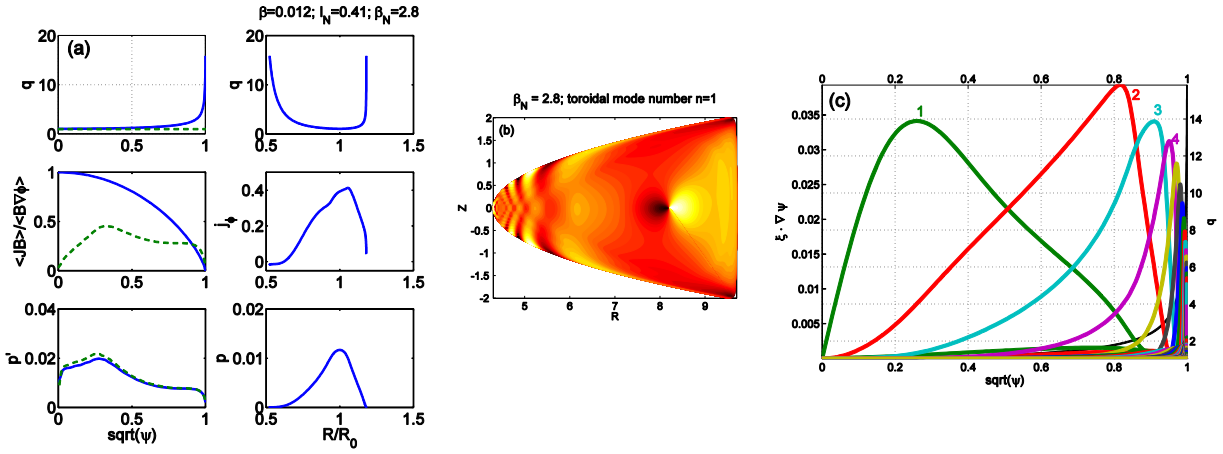

Figure 7. (a) Plasma profiles in the equilibrium with Mercier/ballooning limiting pressure gradient, comet shape, l_i=0.8, (b) and (c) the most unstable n = 1 mode structure, growth rate $\gamma / \omega_A = 0.021$.

For reverse shear q-profiles ballooning/Mercier stable pressure gradients are larger in the negative shear region $\sqrt{\psi} \sim 0.5$ where the magnetic well is re-established (figure 6a). However, large values of p' in the vicinity of the low shear region lead to the destabilization of so-called infernal modes. Approximate bootstrap current alignment with total parallel current density in the core was chosen to limit p' there but was adjusted to the 1st stability limit in the positive shear region resulting in β_N = 3.55, f_{bs} = 1.1 (figure 8a). Rescaling the pressure gradient gives the global n = 1 mode stability with $\beta_N < 2.1$. Note that $q_{min} > 2$ was maintained for better infernal mode stability due to lower normalized current I_N = 0.7. The mode structure is shown in figure 8b and figure 8c.

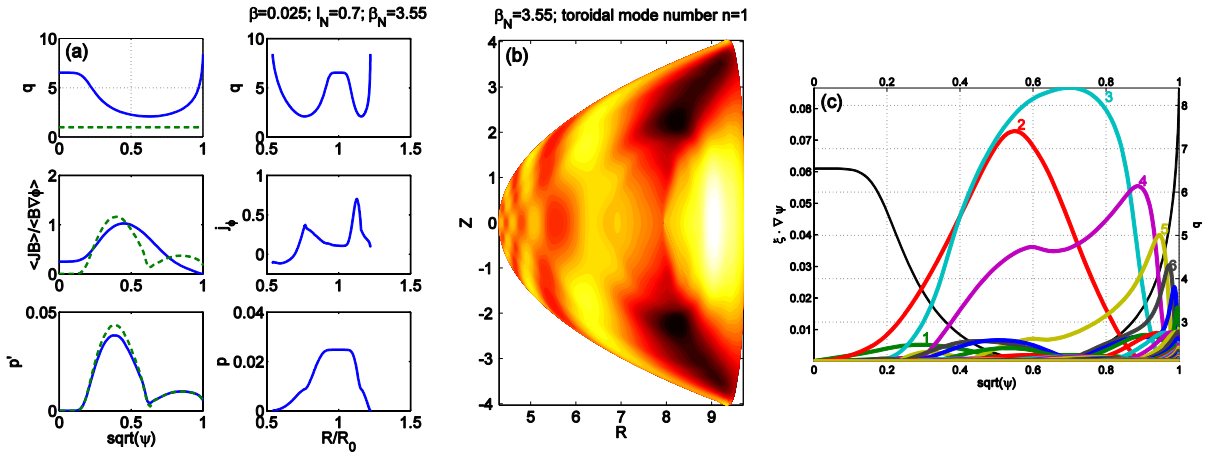

Figure 8. (a) Plasma profiles in the equilibrium with Mercier/ballooning limiting pressure gradient l_i=0.77, reverse shear, (b) and (c) - the most unstable n = 1 mode structure, growth rate $\gamma / \omega_A = 0.041$.

Another interesting feature of low aspect ratio negative triangularity plasmas is significantly lower q_{95} values for the same normalized current I_N because of lower toroidal magnetic field flux $\Phi = \int B_\varphi dS$, $B_\varphi = F_{dia} / R$. In particular, close to the current limit, force-free plasmas with q_{95} below 1 can be stable against external n = 1 kink mode. For the considered configuration with A = 2.6, κ = 1.5, δ = –0.9 the current limit corresponds to I_N ~3, provided that l_i < 0.7 and q_0>0.5 to avoid the internal m/n=1/2

mode instability. However, it does not mean that the maximal normalized current I_N increases for negative triangularity: with the triangularity changed to positive $\delta = 0.9$ the current limit is higher $I_N \sim 4$.

5. Edge stability

The edge kink-ballooning mode stability limits usually follow the changes in the high-*n* limit behavior. Worse localized mode stability leads to lower pressure pedestal height attainable in the negative triangularity configurations and can potentially result in different ELM behaviors for positive and negative triangularity configurations, respectively. Indeed, changing the upper triangularity in TCV plasmas from positive to negative brings an increase in Type I ELM frequency and lower expelled power per ELM [4]. In the negative triangularity double null configuration, higher pedestals can be stable in the 1st ballooning stability region due to high edge shear. Plasma profiles similar to TCV pedestal profiles [30] were used to explore the edge stability limits. In figure 9 edge stability diagrams calculated with the KINX edge stability package including diamagnetic effects are presented. The normalized pressure gradient α and parallel current density $J_{||}/<J>$, where $<J>=I_p/S_p$ is the averaged current density, are estimated at the maximum across the pedestal region. A simple model of the diamagnetic stabilization based on the estimate for the ideal MHD growth rate $\gamma_{MHD} < \omega_*/2$ was used, where ω_* is the ion diamagnetic drift frequency, and the ratio of Alfvén and ion cyclotron frequencies ω_A/ω_{Bi} entering the expression $\omega_*/\omega_A = n(\omega_A/\omega_{Bi})(R_0^2/B)\mu_0 p_i'$, was chosen as for ITER deuterium plasma typical parameters $\omega_A/\omega_{Bi} = 5.2\cdot 10^{-3}$ with the maximal pressure gradient in the pedestal. Note that in fact internal $n \geq 5$ modes set the edge stability limit (compare figure 9a and figure 9b) and diamagnetic stabilization is very inefficient for them. Only low-*n* mode limits significantly change with the free boundary. In contrast to the internal $n > 1$ modes going unstable when the pressure gradient is beyond the ballooning limit in the region with relatively high shear in the middle of the plasma (section 4), the edge modes go unstable in Mercier unstable regime due to low shear in the pedestal with large bootstrap current. Typically there are several unstable modes for each toroidal mode number *n* (figure 10).

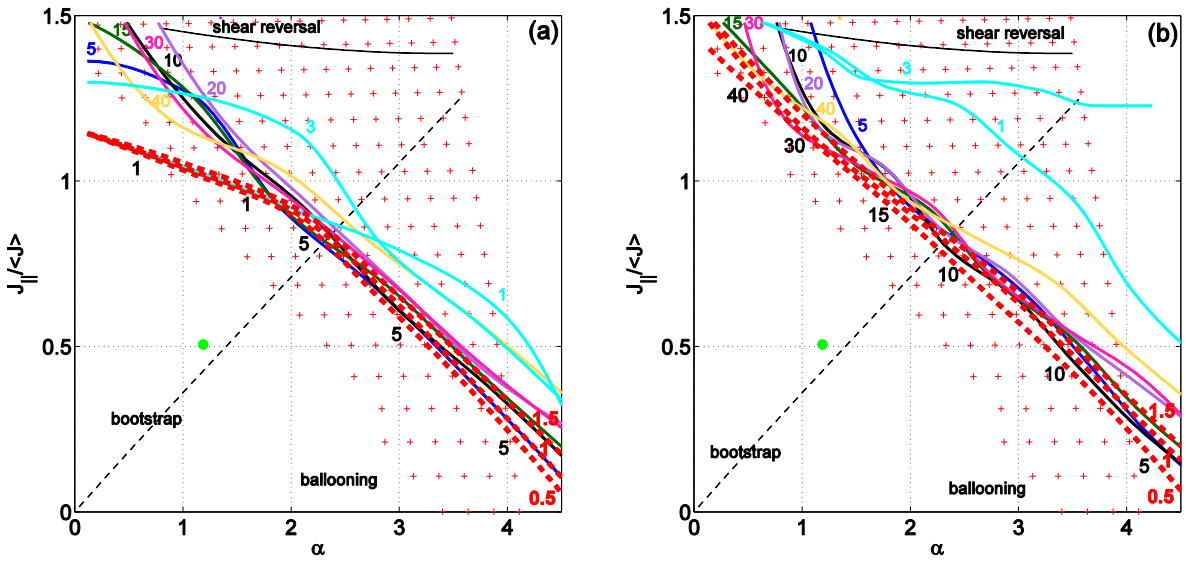

Figure 9. Edge stability diagrams for the negative triangularity double null plasma; normalized pressure gradient α and parallel current density $J_{||}/<J>$ are estimated at the maximum across pedestal region at $\sqrt{\psi} = 0.984$. The ratios of the edge to the maximal values of pressure gradient and parallel current density are 0.48. (a) Free boundary and (b) fixed boundary cases. Green circle

corresponds to initial pedestal parameters. Thick red dashed lines show $\gamma/(\omega_*/2)=0.5,1.0,1.5$ level lines for the most unstable mode, color solid lines show $\gamma/(\omega_*/2)=1$ limits for modes with individual toroidal mode numbers, the most unstable mode numbers are also given along the stability boundary, red crosses mark ballooning/Mercier instability.

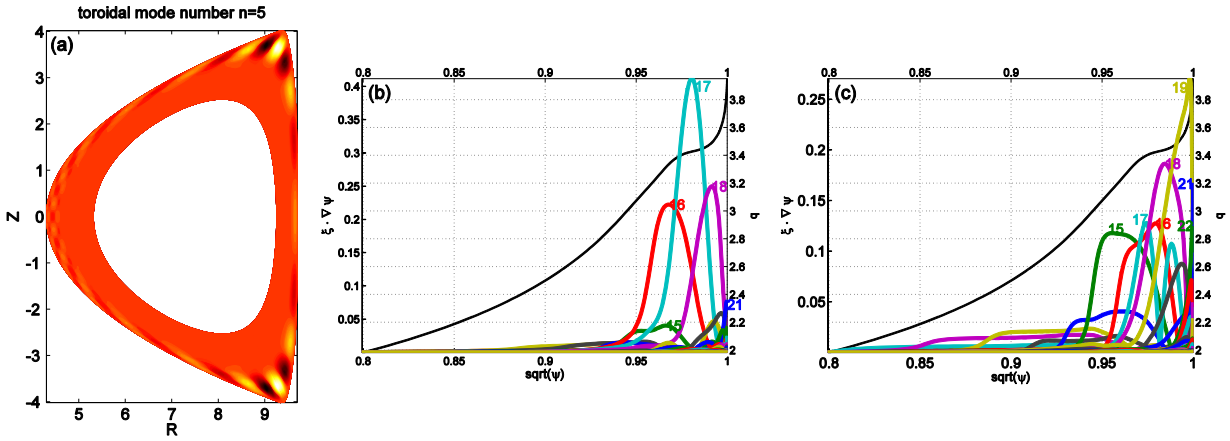

Figure 10. Unstable modes for α = 2.72, $J_{||}/<J>$=1.16. (a) and (b) most unstable n = 5 mode structure shown for $\sqrt{\psi}\geq 0.8$, growth rate $\gamma/\omega_A=0.067$; (c) SFL harmonics of the normal plasma displacement for the second unstable mode, growth rate $\gamma/\omega_A=0.032$. The absolute values of the complex amplitudes are shown.

For comparison the edge stability diagram for a typical single null TCV equilibrium with positive triangularity is shown in figure 11a. For the plasma parameters R_0 = 0.88 *m*, *a* = 0.22 *m* (*A* = 4), κ = 1.75, $\delta_{up}/\delta_{down}$ = 0.05/0.86, *B* =1.4 *T*, I_p = 0.3 *MA*, β_N =1.1, $n_e=3.5\cdot10^{19}\,m^{-3}$ the ratio of Alfvén and ion cyclotron frequencies is $\omega_A/\omega_{Bi}=6.2\cdot10^{-2}$. Assuming $p_i'=p'$ leads to unrealistically strong diamagnetic stabilization governed by $\gamma_{MHD}<\omega_*/2$ due to low ion pressure, and only 5 times lower thresholds, which correspond to the ion pressure 4 times lower than the electron pressure, seems to provide experimentally relevant stability limits. The peeling-ballooning mode structure is presented in figures 11b and 11c. For high edge current density $J_{edge}/J_{||}$ = 0.42 (the parallel current density profile is the same as in figure 3a) the coupling to the peeling mode is quite strong and the maximum of normal displacement is reached at the edge in contrast to the most unstable mode in the negative triangularity equilibrium with the displacement being maximal at the maximum pressure gradient location in the pedestal (figure 10b).

Comparison of the α limits at low values of current density for double null negative triangularity (figure 9a) and positive triangularity (figure 11a) cases shows significantly higher pressure gradient set by high-*n* ballooning modes in the 1st stability region due to high edge shear. Note that the diamagnetic stabilization leads to a significant increase of the pressure gradient in the 1st stability region for the positive shear case in contrast to the edge stability diagrams for the negative triangularity equilibrium in figure 9. The distance between the level lines of the normalized growth rate $\gamma/(\omega_*/2)=0.1,0.2,0.3$ in the parametric plane (thick dashed lines) is much larger as compared to the negative triangularity case which corresponds to much slower increase of the growth rates of the most unstable modes with increasing pedestal height due to the effect of the 2nd stability access for ballooning modes. However electron drift acoustic wave effect can lead to cancellation of the stabilizing ion diamagnetic drift effect and result in the pressure gradient limits approaching that of high-*n* ideal ballooning mode (crosses) in the stability diagram [34]. Sheared plasma rotation in the pedestal might also destabilize high-*n* modes [35].

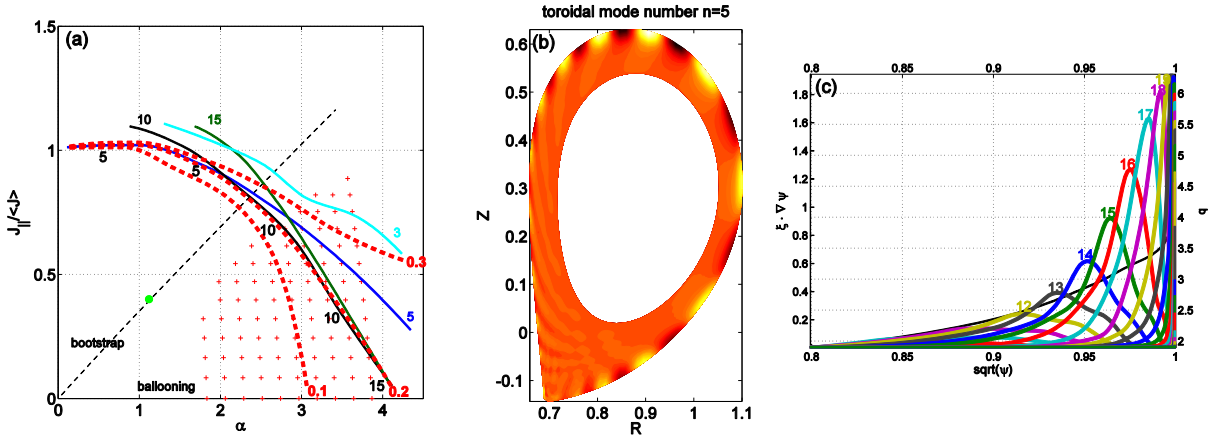

Figure 11. Edge stability diagram for free boundary TCV single null plasma (a): thick red dashed lines show $\gamma/(\omega_*/2) = 0.1, 0.2, 0.3$ level lines for the most unstable mode, color solid lines show $\gamma/(\omega_*/2) = 0.2$ limits for modes with individual toroidal mode numbers, the most unstable mode numbers are also given along the stability boundary. (b) and (c): n=5 mode structure for α = 2.63, $J_{||}/<J>$ =0.93, growth rate $\gamma/\omega_A = 0.083$.

6. Axisymmetric stability

The vertical stability of elongated TCV plasmas with different combinations of positive and negative upper/lower elongations was investigated in [6]. The negative/negative triangulation was found to be the most unstable case with the proximity to the outer vacuum vessel wall being a critical parameter for stability.

Plasma vertical control should be investigated for negative triangularity double null configurations. Even for moderate elongation κ = 1.5, a conducting wall at $a_w/a < 1.25$ is needed to provide ideal $n = 0$ stability for an equilibrium with $l_i = 0.9$, $\beta_N = 3.4$. With 6 cm thick steel wall at $a_w/a = 1.2$, the corresponding $n = 0$ growth rate is 95 s^{-1} (figure 12a) and active feedback control should be assessed. In accordance with the result for the TCV tokamak [6] the proximity of plasma to the LFS wall is a critical parameter for the vertical stability of negative triangularity plasmas, and, in principle, good conducting outer wall alone, located close to the plasma, can provide the vertical stabilization. The $n = 0$ stability looks better for oblate comet shape plasmas: the ideal wall limit is $a_w/a < 1.6$ for $l_i = 0.8$, $\beta_N = 2.8$. However, there are two unstable modes featuring mainly vertical and horizontal plasma displacements with growth rates 12 s^{-1} and 8 s^{-1} (the value of adiabatic index Γ=5/3 matters for the case with up-down symmetric normal displacement), respectively, for the same resistivity wall with $a_w/a = 1.2$ (figures 12b and 12c).

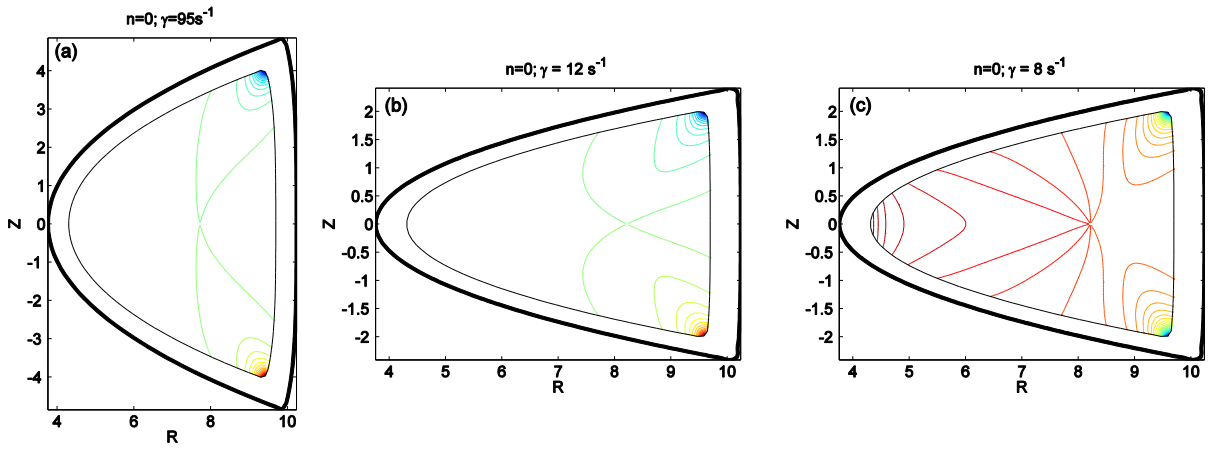

Figure 12. Level lines of the normal plasma displacement for n=0 modes: (a) elongated cross-section (b) "vertical" mode for oblate cross-section and (c) "horizontal" mode for oblate cross-section.

7. Discussion and conclusions

Negative triangularity tokamak configurations with optimized pressure gradient profiles can be stable for reactor relevant values of normalized beta $\beta_N > 3$. Wall stabilization is very inefficient due to strong coupling between internal and external kink modes. Reverse shear configurations allow for larger pressure gradient in the core and larger bootstrap current fraction but coupling to infernal modes leads to lower $\beta_N \sim 2$ and further profile optimization is needed.

Pressure profile in the core might not be limited by localized Mercier modes. It opens more freedom for plasma profile optimization with better bootstrap alignment of parallel current density and possibly larger bootstrap current fraction, but hardly results in enhancement of low-n external kink stability limits beyond the cases with optimized and relatively flat pressure profiles.

Internal modes (unstable already with fixed boundary condition but localized in the pedestal region) set the pedestal height limit, which is much less sensitive to diamagnetic stabilization and pedestal profile variations than conventional peeling-ballooning modes. Double null negative triangularity configurations feature quite high stable pedestals in the 1st region of ballooning stability provided that pedestal current density is low. Though these results from linear MHD theory imply changes in the ELM characteristics as compared to positive triangularity configurations, nonlinear studies are really needed. In order to achieve a soft edge beta limit there is also the need to understand Mercier mode turbulence – a kind of ideal interchange electromagnetic turbulence.

The n=0 stability optimization for the negative triangularity tokamaks is also an interesting subject to investigate since the mode is not rigid. An option of placing additional passive stabilizing plates close to plasma at the LFS side should be considered as the wall position at $a_w - a = 0.2a = 0.54$ cm is only marginal for shielding.

The TCV tokamak with very flexible plasma shape control is very well suited for negative triangularity plasma experiments covering the whole range of principal problems related to the confinement, ELM regimes, scrape-off layer thickness and vertical stability control [4-5], [8]. Together with supporting experiments from other machines and integrated modeling of reactor relevant scenarios, new experimental campaigns on TCV would provide a substantial ground for the negative triangularity tokamak as innovative confinement concept.

With the theoretical predictions supported by an experiment, a negative triangularity tokamak would become a perspective fusion energy system with other advantages including larger separatrix wetted area, more flexible divertor configuration design, wider trapped particle free SOL, lower background magnetic field for internal poloidal field coils and larger pumping conductance from the divertor room. The experimental evidence of the confinement enhancement in negative triangularity plasmas [5,11] provide a ground for optimism in reaching the reactor relevant normalized beta values $\beta_N > 3$. Bridging the central plasma conditions needed for fusion burning to the associated edge plasma properties would require more theoretical and experimental investigations of both the core and the edge plasma performance as well as reactor studies for negative triangularity tokamaks. In particular, a study of radiation shielding performance for a superconducting magnet system with internal poloidal field coils, e.g. as for the helical DEMO reactor [36], would be needed.

References

[1] Kikuchi M and Takizuka T 2013 *Plenary talk US-EU TTF 2013 Santa Rosa (USA) April 9-12, 2013* http://ttf2013.ucsd.edu/TTF_Meeting/Presentations.html

[2] Kikuchi M, Takizuka T and Furukawa M 2014 *JPS Conf. Proc.* **1** 015014

[3] Kikuchi M, Fasoli A, Takizuka T, Diamond P, Duan X, Zushi H, Furukawa M, Kishimoto H, Wu Y, Medvedev S *et al* 2014 *1st International E-Conference on Energies 2014 E002 DOI:10.3390/ECE-1-E002* http://www.sciforum.net/conference/ece-1/paper/2321
[4] Pochelon A, Angelino P, Behn R, Brunner S, Coda S, Kirneva N, Medvedev S Yu, Reimerdes H, Rossel J, Sauter O *et al* 2012 *Plasma and Fusion Research* **7** 2502148
[5] Sauter O, Brunner S, Kim D, Merlo G, Behn R, Camenen Y, Coda S, Duval B P, Federspiel L, Goodman T P *et al* 2014 *Phys. Plasmas* **21** 055906
[6] Medvedev S Yu, Ivanov A A, Martynov A A, Poshekhonov Yu Yu, Behn R, Martin Y R, Pochelon A, Sauter O and Villard L 2008 *Proc. 35th EPS Conf. on Plasma Physics* ECA Vol.32D, P1.072
[7] Medvedev S Yu, Ivanov A A, Martynov A A, Poshekhonov Yu Yu, Martin Y R, Piras F, Pitzschke A, Pochelon A, Sauter O, Villard L and the TCV team 2009 *Proc. 36th EPS Conf. on Plasma Physics* ECA Vol.33E, P2.143
[8] Medvedev S Yu, Ivanov A A, Martynov A A, Poshekhonov Yu Yu, Kikuchi M, Pochelon A, Reimerdes H, Sauter O and Villard L 2014 *Proc. 41th EPS Conf. on Plasma Physics* ECA Vol.38F, P4.039
[9] Kesner J, Ramos J J and Gang F-Y 1995 *Journal of Fusion Energy* **14** 361
[10] Watanabe K Y, Sakakibara S, Narushima Y, Funaba H, Narihara K, Tanaka K, Yamaguchi T, Toi K, Ohdachi S, Kaneko O *et al* 2005 *Nuclear Fusion* **45** 1247
[11] Camenen Y, Pochelon A, Behn R, Bottino A, Bortolon A, Coda S, Karpushov A, Sauter O, Zhuang G and the TCV team 2007 *Nuclear Fusion* **47** 510
[12] Marinoni A, Brunner S, Camenen Y, Coda S, Graves Y P, Lapillonne X, Pochelon A, Sauter O and Villard L 2009 *Plasma Phys. Contr. Fusion* **51** 055016
[13] Kikuchi M, Conn R W, Najmabadi F, Seki Y 1991 *Fusion Engineering and Design* **16** 253
[14] Ueda N, Tanaka M, Kikuchi M, Seki Y 1992 *Nuclear Fusion* **32** 253
[15] Ryutov D D 2007 *Phys. Plasmas* **14** 064502
[16] Ryutov D D, Cohen R H, Rognlien T D, Umansky M V 2008 *Phys. Plasmas* **15** 092501
[17] Asakura N, Shinya K, Tobita K, Hoshino K, Shimizu K, Uto H, Someya Y, Nakamura M, Ono N, Kobayashi M, Tanaka H 2013 *Trans. Fusion Science and Technology* **63** 70
[18] Evans T E, Moyer R A, Watkins J G, Osborne T H, Thomas P R, Becoulet M, Boedo J A, Doyle E J, Fenstermacher M E, Finken K H *et al* 2005 *Nuclear Fusion* **45** 595
[19] Lang P T, Conway G D, Eich T, Fattorini L, Gruber O, Günter S, Horton L D, Kalvin S, Kallenbach A, Kaufmann M *et al* 2004 *Nuclear Fusion* **44** 665
[20] Kirk A, Harrison J, Liu Yueqiang, Nardon E, Chapman I T and Denner P 2012 *Phys. Rev. Lett.* **108** 255003
[21] Freidberg J P 1987 *Ideal Magneto-Hydro-Dynamics* Plenum, New York
[22] Mercier C 1960 *Nucl. Fusion* **1** 47
[23] Wilson H R and Miller R L 1999 *Phys. Plasmas* **6** 873
[24] Solev'ev L S, Shafranov V D and Yurchenko E I 1968 *Plasma Physics and Controlled Nuclear Fusion Research (IAEA, Vienna)* vol.1**,** p.175 (1969 *Nuclear Fusion Suppl.* p.251)
[25] Pogutse O P and Yurchenko E I 1986 *Reviews Of Plasma Physics* vol.11 Edited by M.A.Leontovich, Consultants Bureau, New York, 1982 Russian Original Atomizdat, Moscow
[26] Drozdov V V 2014 *Private communication* March 2014
[27] Degtyarev L M, Drozdov V V, Martynov A A, Medvedev S Yu 1985 On the tokamak beta-values limited by ideal MHD-stability *Proc. Int. Conf. on Plasma Physics* Lausanne (Switzerland), 27 Jun - 3 Jul 1984, EUR-9708 (V.1), p. 157-175
1985 *Fizika Plazmy* **11** 1299-1310 (in Russian, for English translation see *The Soviet Journal of Plasma Physics*)
[28] Connor J W, Hastie R J and Taylor J B 1979 *Proc. R. Soc. Lond.* A. **365** 1-17
[29] Degtyarev L, Martynov A, Medvedev S, Troyon F, Villard L, Gruber R 1997 *Comput. Phys. Comm.* **103** 10
[30] Behn R, Alfier A, Medvedev S Yu, Zhuang Ge, Pasqualotto R, Nielsen P, Martin Y and the TCV team 2007 *Plasma Phys. Control. Fusion* **49** 1289
[31] Porcelli F, Rosenbluth M N 1998 *Plasma Phys. Control. Fusion* **40** 481

[32] Ohkawa T, Chan V S, Chu M S, Dominguez R R and Miller R L 1988 *Plasma Physics and Controlled Nuclear Fusion Research (IAEA, Vienna)* IAEA-CN-50/E-III-7 (1989 *Nuclear Fusion Suppl.* vol.1, p.681)
[33] Hsu S C, Artun M and Cowley S C 1996 *Phys. Plasmas* **3** 266
[34] Aiba N and Oyama N 2012 *Nucl. Fusion* **52** 114002
[35] Aiba N, Tokuda S, Furukawa M, Oyama N and Ozeki T 2009 *Nucl. Fusion* **49** 065015
[36] Sagara A, Goto T, Miyazawa J, Yanagi N, Tanaka T, Tamura H, Sakamoto R, Tanaka M, Tsumori K, Mitarai O *et al* 2012 *Fusion Engineering and Design* **87** 594